Schweizerischer Erdbebendienst
Service Sismologique Suisse
Servizio Sismico Svizzero
Servizi da Terratrembels Svizzer

ETH
Eidgenössische Technische Hochschule Zürich
Swiss Federal Institute of Technology Zurich

Chur - Gewerbeschule (SCUG)

SITE CHARACTERIZATION REPORT

Clotaire MICHEL, Daniel ROTEN, Carlo CAUZZI

Valerio POGGI, Jan BURJANEK, Donat FÄH

Sonneggstrasse 5 CH-8092 Zürich Switzerland; E-mail: clotaire.michel@sed.ethz.ch

Last modified : November 5, 2013

Abstract

Ambient vibration array measurements were performed in the Rhine basin in Chur. The new station SCUG of the Swiss Strong Motion Network located in the Chur cite centre is replacing the dial-up station SCUT. In order to characterize the velocity profile under the station, single station and array measurements with a $500\,\mathrm{m}$ aperture were performed. The H/V survey and polarization analysis showed that the Rhine basin in Chur behaves in a 2D fashion and that SCUG station is located on the deepest part with a fundamental frequency at $0.46\,\mathrm{Hz}$. The array measurements presented in this study allowed to derive a velocity model below the SCUG station. We found a velocity profile with a strong gradient in the first $30\,\mathrm{m}$ from $300-400\,\mathrm{m/s}$ to approximately $1000\,\mathrm{m/s}$ at $30\,\mathrm{m}$. Below the velocity is increasing up to $1500-2000\,\mathrm{m/s}$ down to the bedrock. The bedrock depth is not well constrained at $600-800\,\mathrm{m}$ ($650\,\mathrm{m}$ according to the literature), much below the constrained part of the profile that reaches $180\,\mathrm{m}$. $V_{s,30}$ is found to be around $714\,\mathrm{m/s}$, which is much higher than expected in the Rhine valley. The theoretical SH transfer function and impedance contrast of the quarter-wavelength velocity computed from the inverted profiles support a slightly increasing amplification with frequency with amplitude keeping between 2 and 3. This inversion is not satisfactory because not enough information is available to constrain the deeper part of the profiles, absolutely necessary to reproduce the observed dispersion. Comparison with transfer functions from earthquakes suggests that the profiles may be more complex at depth (velocity inversion?) and can therefore not be simply fixed. In order to improve this, a larger array and/or other measurement types should be used.

Contents

1 Introduction

The station SCUG (Chur Gewerbeschule) is part of the Swiss Strong Motion Network (SSMNet) in the Graubünden. SCUG has been installed in the framework of the SSMNet Renewal project in 2011, replacing the SCUT (Chur Tittwiesenstrasse) dial-up station. This project includes also the site characterization. The passive array measurement has been selected as a standard tool to investigate these sites. Such a measurement campaign was carried out on 21st October 2011 in the Gewerbeschule Daleu in Chur (Fig. 1), with centre at station SCUG, in order to characterize the soil column under this station. According to the geological map, this station is located on the loose alluvia of the Rhine valley. Moreover, single station measurements in several points were performed in the whole city of Chur in October 26th-28th 2010 and December 22th 2010 by I. Egger, as well as one week test measurements at some sites. The H/V spectral ratios were computed, in order to map the resonance frequency in the city. This report presents the measurement setups, the results of the H/V analysis and of the array processing of the surface waves (dispersion curves). Then, an inversion of these results for a velocity profile is performed. Standard parameters are derived to evaluate the amplification at this site.

Canton	City	Location	Station code	Site type	Slope
Graubünden	Chur	Gewerbeschule	SCUG	Deep sediments	Flat

Table 1: Main characteristics of the study-site.

Figure 1: Picture of the site.

2 Geology

Preusser et al. [2010] propose a cross-section of the Rhine valley in Chur. According to their sketch (Fig. 2), station SCUG is located in the deepest part of the valley, with a depth of approximately $650\,\mathrm{m}$.

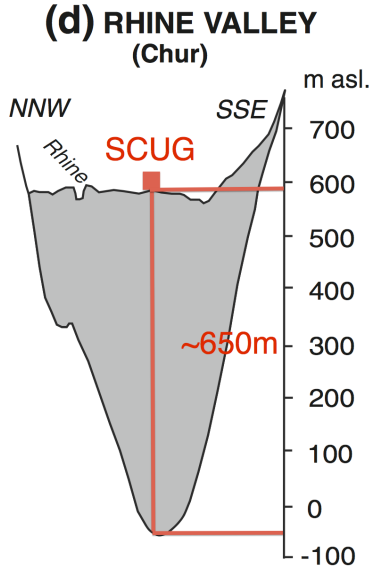

Figure 2: Cross-section of the Rhine valley in Chur (vertical exaggeration of 5) and position of station SCUG. Adapted from Preusser et al. [2010].

3 Experiment description

3.1 Ambient Vibrations

The ground surface is permanently subjected to ambient vibrations due to:

- natural sources (ocean and large-scale atmospheric phenomena) below $1\,\mathrm{Hz}$,
- local meteorological conditions (wind and rain) at frequencies around $1\,\mathrm{Hz}$,
- human activities (industrial machines, traffic…) at frequencies above $1\,\mathrm{Hz}$ [Bonnefoy-Claudet et al., 2006].

The objective of the measurements is to record these ambient vibrations and to use their propagation properties to infer the underground structure. First, the polarization of the recorded waves (H/V ratio) is used to derive the resonance frequencies of the soil column. Second, the arrival time delays at many different stations are used to derive the velocity of surface waves at different frequencies (dispersion). The information (H/V, dispersion curves) is then used to derive the properties of the soil column using an inversion process.

3.2 Equipment

For the array measurements, 11 Quanterra Q330 dataloggers named NR01 to NR12 (except NR06) and 14 Lennartz 3C 5 s seismometers were available (see Tab. 2). Each datalogger can record on 2 ports A (channels EH1, EH2, EH3 for Z, N, E directions) and B (channels EH4, EH5, EH6 for Z, N, E directions). Time synchronization was ensured by GPS. The sensor were placed on a metal tripod in a $20\,\mathrm{cm}$ deep hole, when possible, for better coupling with the ground.

For the single station measurements, 1 Nanometrics Taurus datalogger and 1 Lennartz 3C 5 s seismometer were used for the first dataset, whereas for the second measurement, Quanterra Q330 datalogger with Lennartz 3C 5 s seismometer were used (see Tab. 2). The time stamps was not synchronized on GPS and may suffer from a shift of several seconds (or more). The sensor is placed directly on the ground (generally road) and leveled using the screws. A laptop with a seedlink server could be linked to the datalogger to stream the data to the computer. They could therefore be read by the Geopsy software `http://www.geopsy.org` and the processing made in near real-time. It was therefore possible to have an idea of the results directly on the field, refine the measurement grid where it was necessary, record more time if necessary etc.

Digitizer	**Model**	**Number**	**Resolution**
	Quanterra Q330	11	24 bits
	Nanometrics Taurus	1	24 bits
	Quanterra Q330	1	24 bits
Sensor type	**Model**	**Number**	**Cut-off frequency**
Velocimeter	Lennartz 3C	14	0.2 Hz
Velocimeter	Lennartz 3C	1	0.2 Hz

Table 2: Equipment used.

3.3 Geometry of the arrays

Two array configurations were used, for a total of 5 rings of 15, 30, 60, 120 and $250\,\mathrm{m}$ radius around a central station. The first configuration includes the 3 inner rings with 14 sensors; the second configuration includes the 2 outer rings (plus the central station) with 11 sensors. The minimum inter-station distance and the aperture are therefore 15 and $120\,\mathrm{m}$ and 120 and $500\,\mathrm{m}$, respectively. The experimental setup is displayed in Fig. 3. The final usable datasets are detailed in section 4.2.

For the single station measurements, a cross-section of the Rhine valley as well as a denser grid in the old city (alluvial fan) were intended to be performed, whereas at the end only few points gave reliable results (Fig. 4). The final datasets are detailed in section 4.2, without considerations about the recording quality.

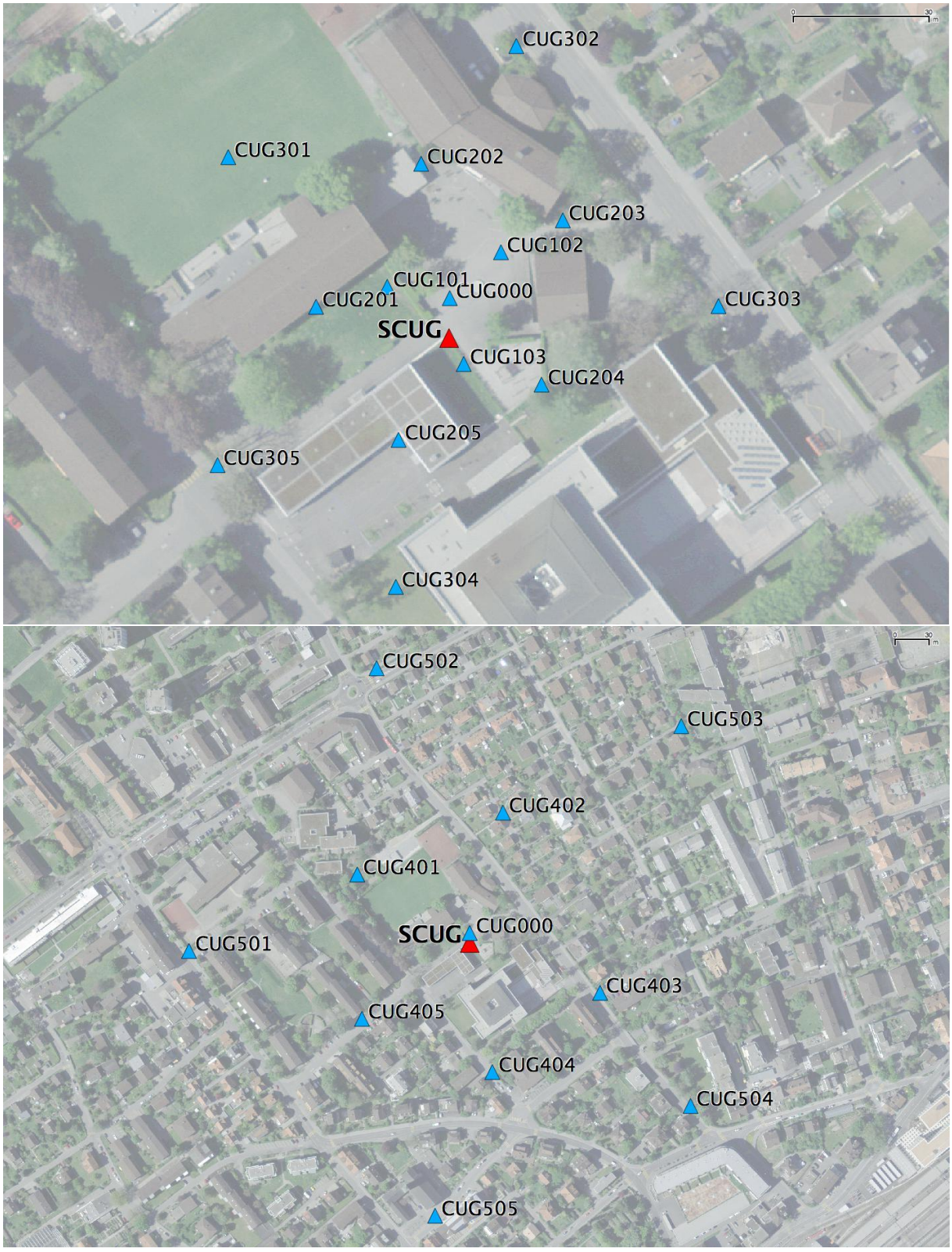

Figure 3: Geometry of the arrays (configuration 1 (top) and configuration 2 (bottom).

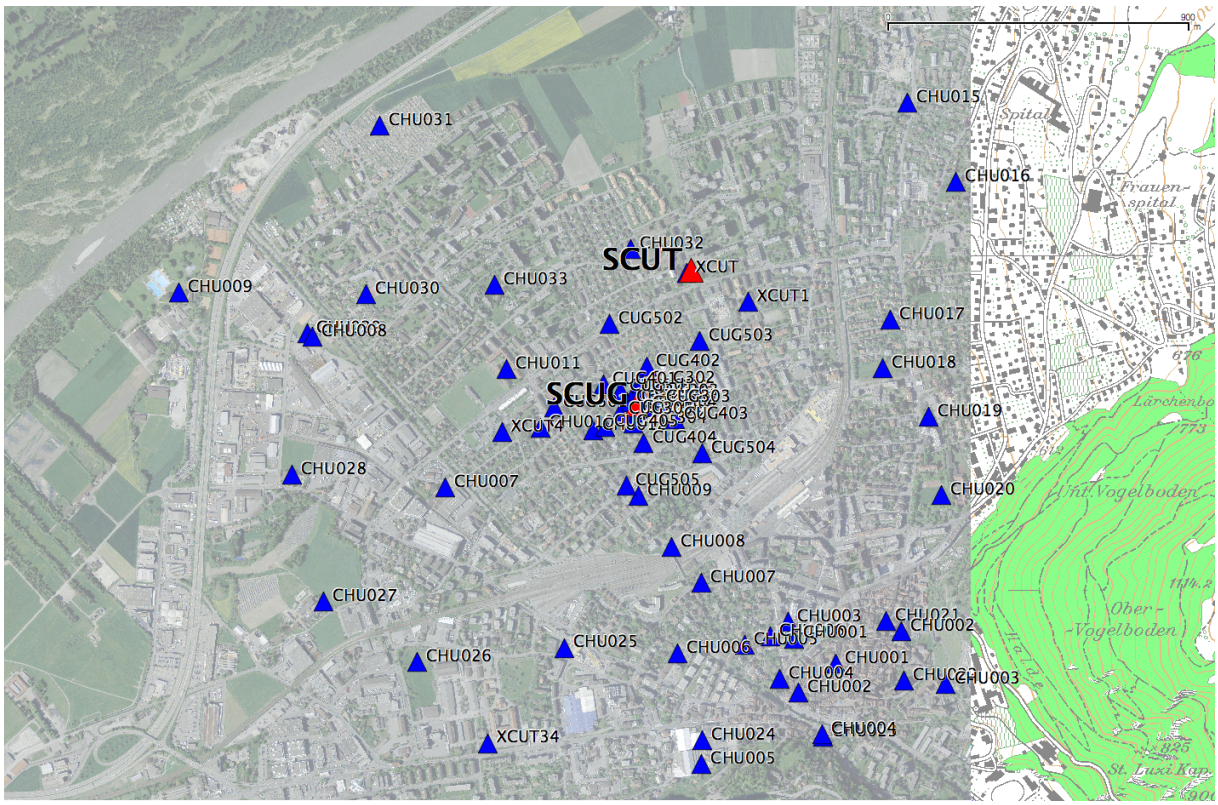

Figure 4: All recordings available in Chur (blue) and permanent stations (red).

3.4 Positioning of the stations

For the array data, the sensor coordinates were measured using a differential GPS device (Leica Viva), including only a rover station and using the Real Time Kinematic technique provided by Swisstopo. It allows an absolute positioning with an accuracy of about 3 cm on the Swissgrid. However, the system did not work for some points too close to buildings. For the others, around 10 minutes GPS recordings were performed and post-processed using a virtual reference provided by Swisstopo (RINEX data) and the LGO software. The accuracy of location is variable but better than 30 cm in this case, except for point CUG205 that is wrongly positioned. It was located by hand on the Swissimage with an accuracy of 50 cm.

For the single station measurement, the positioning of the stations was done by picking points on the 1/25000 Swisstopo map. It allows a positioning with an accuracy of about 5 m.

4 Data quality

4.1 Usable data

The largest time windows were extracted, for which all the sensors of the array were in position and the GPS synchronization was ensured. GPS measurement were typically not performed during the data acquisition. Points CUG302, 303, 305, 403, 404, 504 were close to major roads and therefore noisier, point 305 was even kicked during the measurement. Point CUG301 happened to be on top of an underground structure, which can be seen on the horizontal recordings. The second dataset was recorded during the rush hour with a heavier traffic.

For the single station data, the noise level is large on average since the site is located in a city. Moreover, under 1 Hz, most of the recordings appear not to be usable, the reason for this is currently being investigated and is linked to the combination Taurus/Le5s.

The characteristics of the datasets are detailed in Tab. 3.

4.2 Data processing

The data were first converted to SAC format including in the header the sensor coordinates (CH1903 system), the recording component and a name related to the position. The name is made of 3 letters characterizing the location (CUG for the array, CHU for the single station measurements), 1 digit for the ring and 2 more digits for the number in the ring. Recordings were not corrected from the instrument response.

Dataset	Starting Date	Time	Length	F_s	Min. inter-distance	Aperture	# of points
1	2011/10/21	9:03	117 min	200 Hz	15 m	120 m	14
2	2011/10/21	14:34	147 min	200 Hz	120 m	500 m	11
1	2010/08/23	07:45	38 min	200 Hz			1
2	2010/08/23	08:47	41 min	200 Hz			1
3	2010/08/23	10:37	40 min	200 Hz			1
4	2010/08/23	11:34	39 min	200 Hz			1
5	2010/08/23	12:27	35 min	200 Hz			1
6	2010/08/23	13:25	38 min	200 Hz			1
7	2010/08/23	14:26	38 min	200 Hz			1
8	2010/08/23	15:17	33 min	200 Hz			1
9	2010/08/24	08:27	16 min	200 Hz			1
10	2010/08/24	09:29	31 min	200 Hz			1
11	2010/08/24	10:22	27 min	200 Hz			1
12	2010/08/24	11:08	42 min	200 Hz			1
13	2010/08/24	12:23	35 min	200 Hz			1
14	2010/08/24	13:17	29 min	200 Hz			1
15	2010/08/24	14:07	25 min	200 Hz			1
16	2010/08/24	14:46	20 min	200 Hz			1
17	2010/08/25	07:01	34 min	200 Hz			1
18	2010/08/25	07:51	33 min	200 Hz			1
19	2010/08/25	08:40	26 min	200 Hz			1
20	2010/08/25	09:21	35 min	200 Hz			1
21	2010/08/25	11:44	33 min	200 Hz			1
22	2010/08/25	12:36	31 min	200 Hz			1
23	2010/08/25	13:29	29 min	200 Hz			1
24	2010/08/25	14:17	33 min	200 Hz			1
25	2010/08/25	15:13	32 min	200 Hz			1
26	2010/08/25	17:25	23 min	200 Hz			1
27	2010/08/26	07:00	32 min	200 Hz			1
28	2010/08/26	07:49	34 min	200 Hz			1
29	2010/08/26	08:40	34 min	200 Hz			1
30	2010/08/26	09:29	29 min	200 Hz			1

Table 3: Usable datasets.

5 H/V processing

5.1 Processing method and parameters

In order to process the H/V spectral ratios, several codes and methods were used. The classical H/V method was applied using the Geopsy `http://www.geopsy.org` software. In this method, the ratios of the smoothed Fourier Transform of selected time windows are averaged. Tukey windows (cosine taper of 5% width) of $100\,\mathrm{s}$ long overlapping by 50% were selected. Konno and Ohmachi [1998] smoothing procedure with b=60 was used. The classical H/V method of Fäh et al. [2001] was also applied.

Moreover, the time-frequency analysis method [Fäh et al., 2009] was used to estimate the ellipticity function more accurately using the Matlab code of V. Poggi. In this method, the time-frequency analysis using the Wavelet transform is computed for each component. For each frequency, the maxima over time (10 per minute with at least $0.1\,\mathrm{s}$ between each) in the TFA are determined. The Horizontal to Vertical ratio of amplitudes for each maxima is then computed and statistical properties for each frequency are derived. Cosine wavelet with parameter 9 was used. The mean of the distribution for each frequency is stored. For the sake of comparison, the time-frequency analysis of Fäh et al. [2001], based on the spectrogram, was also used, as well as the wavelet-based TFA coded in Geopsy.

The ellipticity extraction using the Capon analysis [Poggi and Fäh, 2010] on the array measurement was also performed (see section 6).

Method	Freq. band	Win. length	Anti-trig.	Overlap	Smoothing
Standard H/V Geopsy	$0.2-20\,\mathrm{Hz}$	$100\,\mathrm{s}$	No	50%	K&O 60
Standard H/V D. Fäh	$0.2-20\,\mathrm{Hz}$	$30\,\mathrm{s}$	No	75%	-
H/V TFA Geopsy	$0.2-20\,\mathrm{Hz}$	Morlet m=8 fi=1	No	-	-
H/V TFA D. Fäh	$0.2-20\,\mathrm{Hz}$	Specgram	No	-	-
H/V TFA V. Poggi	$0.2-20\,\mathrm{Hz}$	Cosine wpar=9	No	-	No

Table 4: Methods and parameters used for the H/V processing.

5.2 Results in the array

H/V curves are consistent for all the recordings in the array (Fig. 5), showing however variability in their quality. Moreover, all the methods to compute H/V ratios are compared on Fig. 6, where the classical methods were divided by $\sqrt{2}$ to correct from Love waves influence [Fäh et al., 2001]. The matching is reasonable considering the parametrization of the codes of D. Fäh were kept with default values and not adapted to low frequency peaks. The 3C FK analysis provides similar results but is not able to explore the part related to the fundamental frequency due to the too small array aperture compared to the basin depth. The peak is relatively clear around $0.46\,\mathrm{Hz}$, with a peak amplitude around 2.5. For some sensors, the coupling was not good enough to well illuminate the peak (e.g. CUG101, CUG203 compared to other points at the centre). As expected, CUG301, that happened to have been installed on an underground

structure does not show any peak. Other stations like CUG404, CUG501, CUG504, CUG505 also do not provide clear peaks. Heavy traffic or bad sensor placement can be reasons for this.

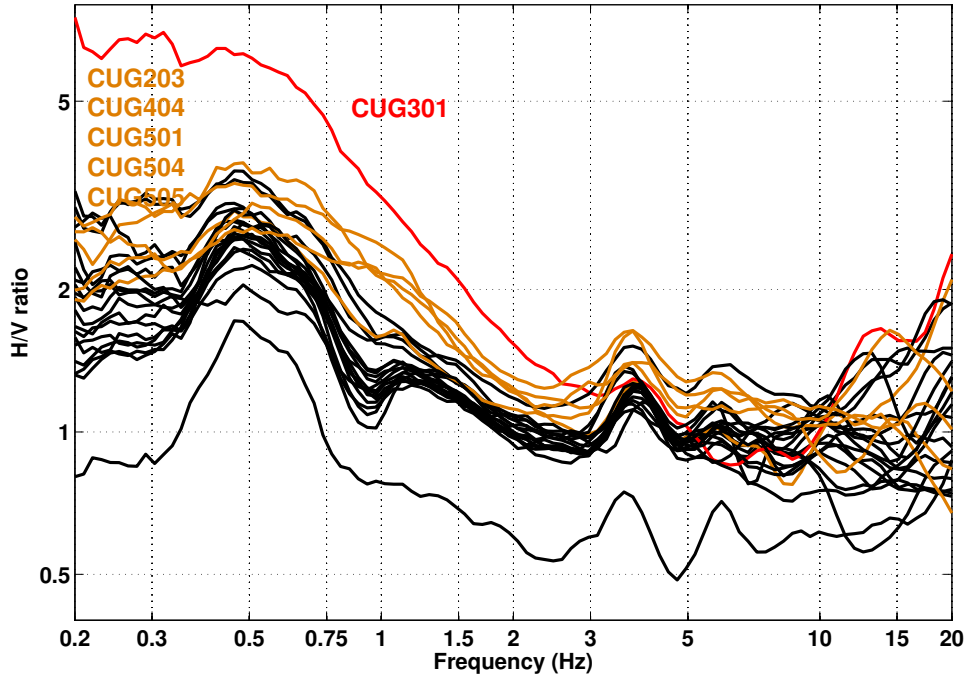

Figure 5: H/V spectral ratios (time-frequency analysis code V. Poggi).

5.3 Results in the whole city

Due the bad quality of a large part of the single station recordings, only few parts of the city are covered by H/V measurements (Fig. 7). These results confirm that station SCUG is located on the deepest part of the basin (Fig. 2) with a frequency of $0.46\,\mathrm{Hz}$. In the old city and on the edges, the frequency increases rapidly. The question is to know whether the frequency in the deep basin represents the 1D resonance of the site or is affected by the 2D resonance of the whole valley.

Bard and Bouchon [1985] proposed a method to predict the observation of 2D resonance in valleys based on the valley shape and the velocity contrast. The valley shape is not very well defined, but one can assume the half-depth width of the valley $2w$ as defined by Roten et al. [2006] to be between 1000 (half of the valley width) and $1400\,\mathrm{m}$ ($1250\,\mathrm{m}$ according to Fig. 2). Therefore the shape ratio $h/2w$ is between 0.4 and 0.8 (0.52 according to Fig. 2). The velocity contrast between sediments and bedrock, considering the array results, seems low between 1 and 2.3, but the bedrock velocity is not constrained. Therefore, according to Fig. 8, the valley is unlikely to show a pure 2D behaviour.

In addition, polarization analysis [Burjánek et al., 2010] was performed on the recordings of dataset 2 of the array measurements to determine if this frequency peak was due to a 2D resonance. Fig. 9 shows a clear SH polarization at $0.5\,\mathrm{Hz}$ in the direction of the valley axis for

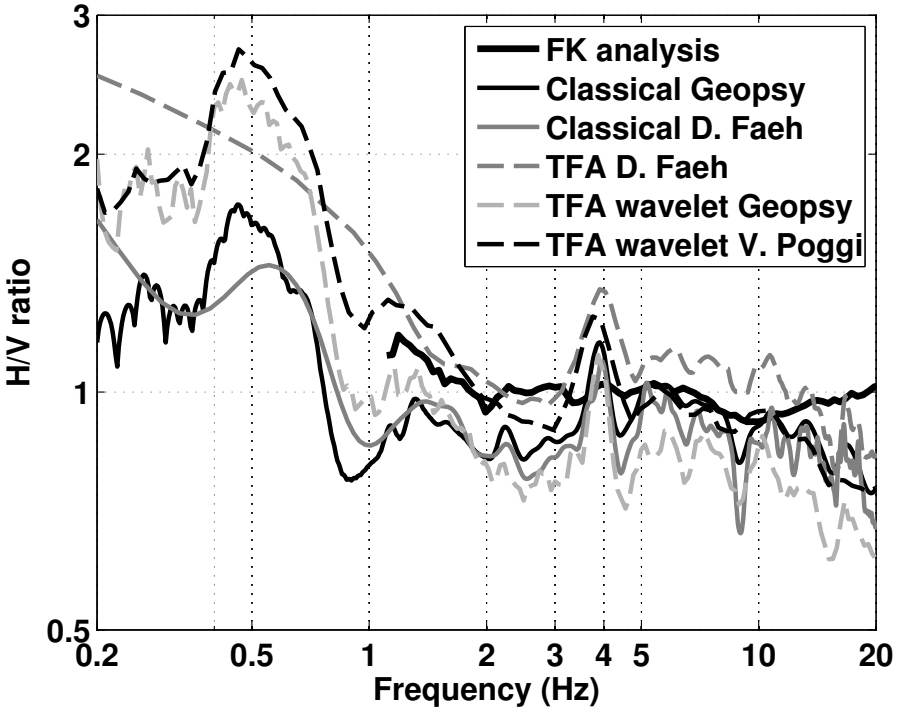

Figure 6: H/V spectral ratios for point CUG000 using the different codes. Classical methods were divided by $\sqrt{2}$.

most of the stations. Despite the theory, this frequency is therefore related to a 2D resonance and should be used in the inversion only with care.

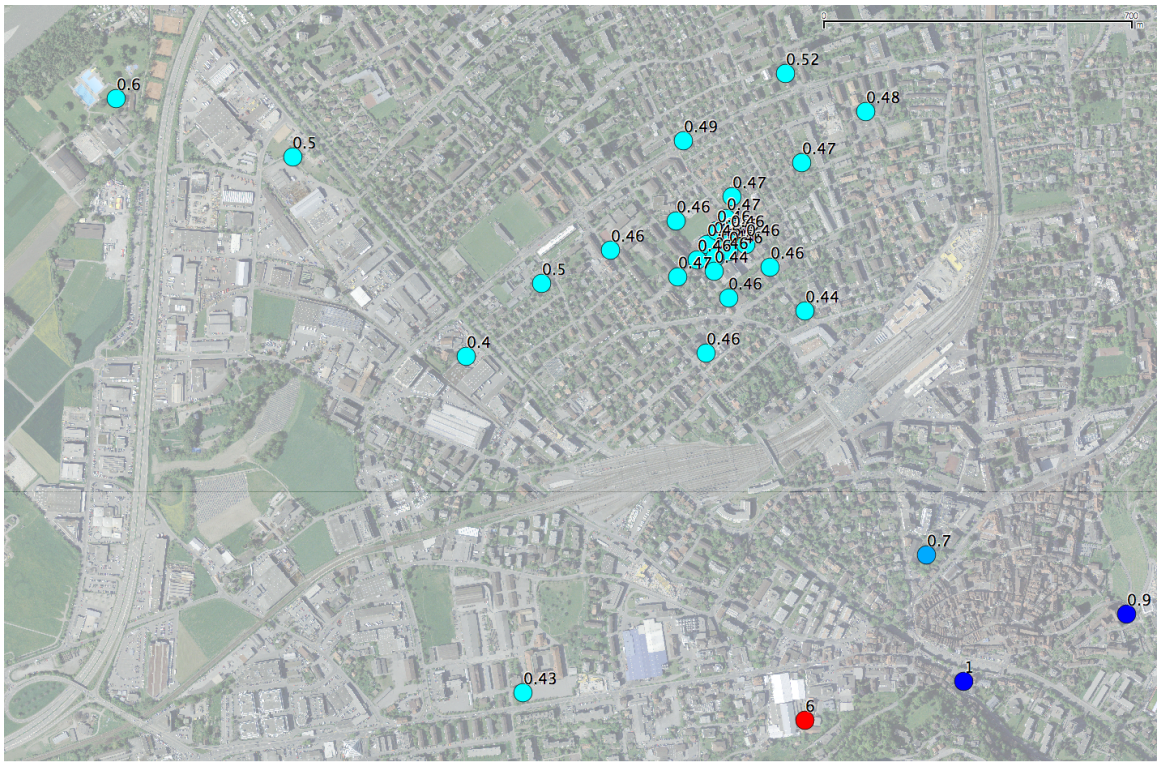

Figure 7: Fundamental frequencies in the city of Chur.

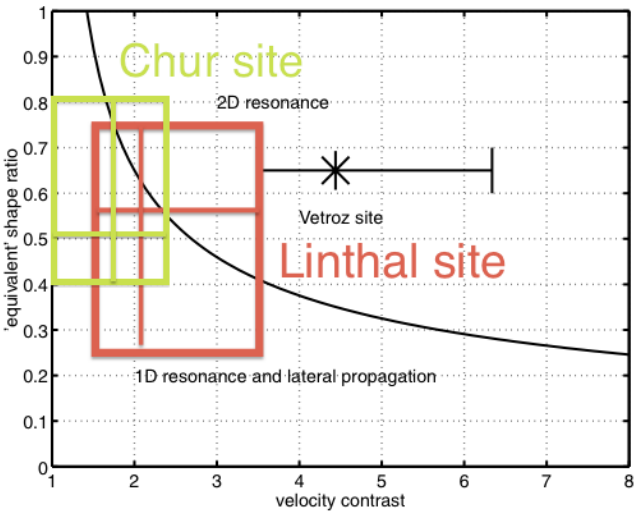

Figure 8: 1D/2D resonance domains for the Chur site and comparisons with the Linthal site and the Rhone valley, modified from Roten et al. [2006]

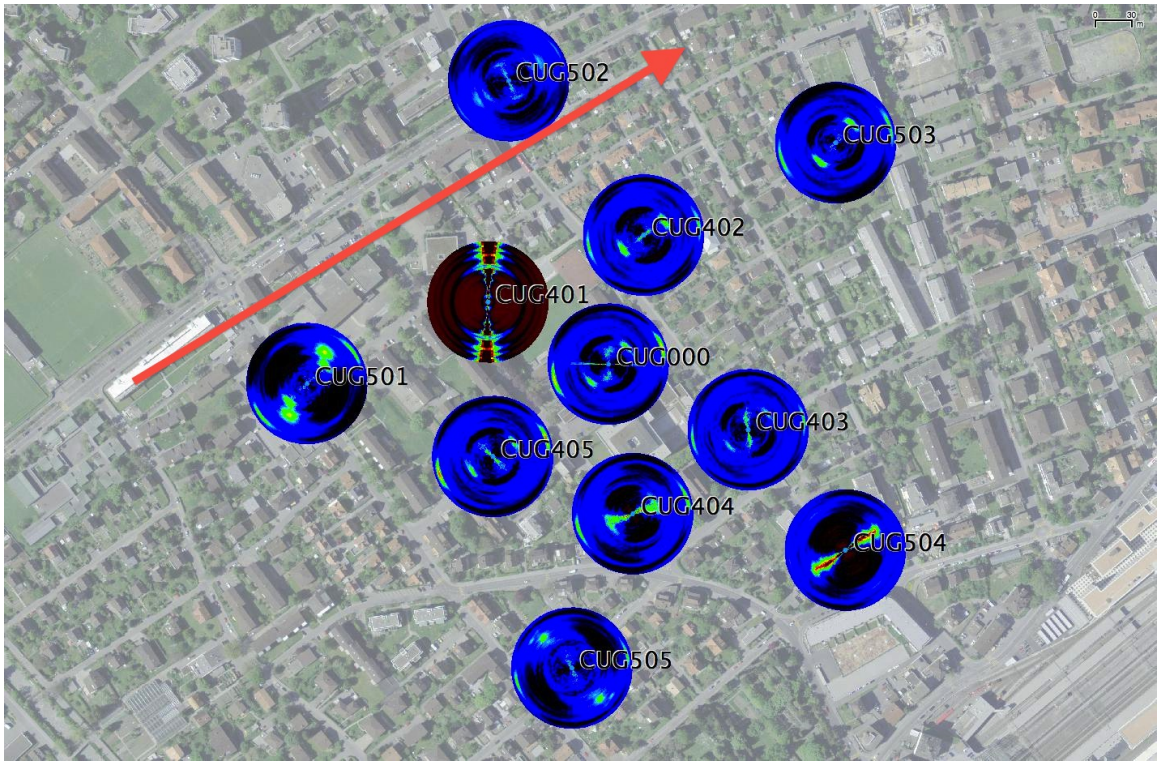

Figure 9: Polarization analysis of the array recordings in Chur. Frequency scale starts at 0.1 Hz in the centre of each circle to 5 Hz at the border. Red arrow corresponds to the valley axis.

6 Array processing

6.1 Processing methods and parameters

The vertical components of the arrays were processed using the FK and the High-resolution FK analysis [Capon, 1969] using the Geopsy `http://www.geopsy.org` software. Better results were obtained using large time windows (300T, where T stands for period). The FK distributions were concatenated.

Moreover, a 3C array analysis [Fäh et al., 2008] was also performed using the array_tool_3C software [Poggi and Fäh, 2010]. The results of computations of both datasets were merged to estimate the dispersion curves. It allows to derive Rayleigh and Love fundamental modes.

Method	Set	Freq. band	Win. length	Anti-trig.	Overlap	Grid step	Grid size	# max.
HRFK 1C	1	$1-30\,\mathrm{Hz}$	$300T$	No	50%	0.001	0.4	5
HRFK 1C	2	$1-30\,\mathrm{Hz}$	$300T$	No	50%	0.001	0.4	5
HRFK 3C	1	$1-30\,\mathrm{Hz}$	Wav. 10	No	50%	300	2000	5
			Tap. 0.2			m/s	m/s	
HRFK 3C	2	$1-30\,\mathrm{Hz}$	Wav. 10	No	50%	300	2000	5
			Tap. 0.2			m/s	m/s	

Table 5: Methods and parameters used for the array processing.

6.2 Obtained dispersion curves

The first mode (Rayleigh) in the 1C FK analysis could be picked between 1.3 and $21.5\,\mathrm{Hz}$ (Fig. 10) including its standard deviation. The dispersion curve close to the lower array limit does not seem reliable. The velocities are ranging from $1280\,\mathrm{m/s}$ at $1.3\,\mathrm{Hz}$ down to $515\,\mathrm{m/s}$ at $21.5\,\mathrm{Hz}$.

Using the 3C component, both fundamental Rayleigh and Love modes can be picked (Fig. 11). The fundamental Rayleigh mode shows no difference with the 1C analysis (Fig. 12). Moreover, the fundamental Rayleigh and Love modes are similar. Rayleigh fundamental mode is picked from 1.4 to $24\,\mathrm{Hz}$ and Love from 1.5 to $21\,\mathrm{Hz}$ (Fig. 12).

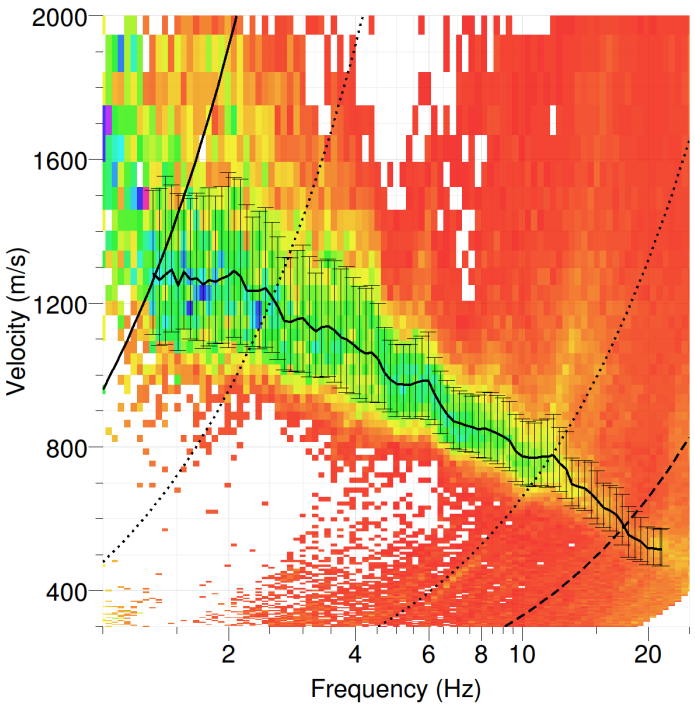

Figure 10: Dispersion curve obtained from the 1C array analysis.

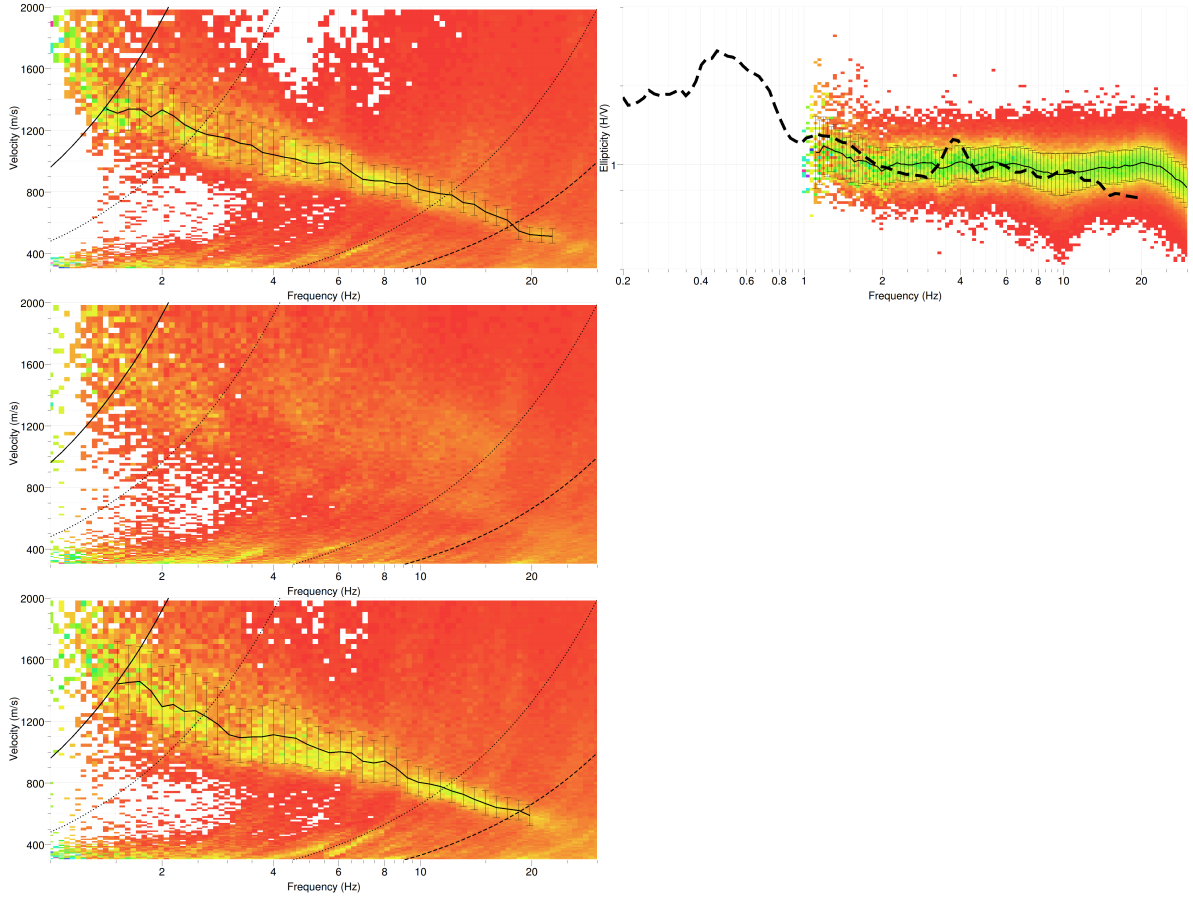

Figure 11: Dispersion curves obtained from the 3C array analysis: vertical direction dispersion and ellipticity (top), radial direction (centre) and transverse direction (bottom).

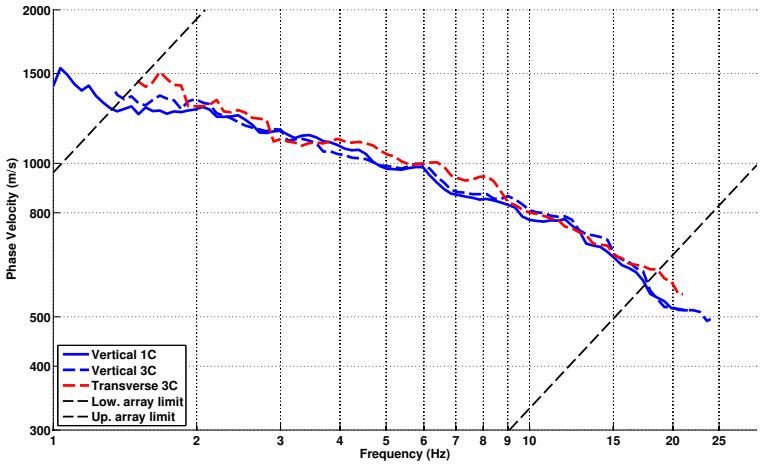

Figure 12: Picked dispersion curves from 1C and 3C analyses.

7 Inversion and interpretation

7.1 Inversion

For the inversion, the Love and Rayleigh fundamental modes (3C analysis) dispersion curves between 1.4 and $23\,\mathrm{Hz}$ were used as simultaneous targets without standard deviation to avoid different weighting as well as the H/V curve segmented into 2 parts: the right flank of the ellipticity (code V. Poggi) with weight 10 between 0.6 and $0.9\,\mathrm{Hz}$ and the ellipticity from 3C FK analysis between 1.3 and $30\,\mathrm{Hz}$. A weight of 0.3 was assigned to the ellipticity information. All curves were resampled using 50 points between 0.2 and $25\,\mathrm{Hz}$ in log scale. Even if the ellipticity information is related to a 2D resonance, it is the only constraint available for the larger depths that are absolutely necessary to reproduce realistic amplification functions.

The inversion was performed using the Improved Neighborhood Algorithm (NA) [Wathelet, 2008] implemented in the Dinver software. In this algorithm, the tuning parameters are the following: Ns_0 is the number of starting models, randomly distributed in the parameter space, Nr is the the number of best cells considered around these Ns_0 models, Ns is the number of new cells generated in the neighborhood of the Nr cells (Ns/Nr per cell) and It_{max} is the number of iteration of this process. The process ends with $Ns_0 + Nr * \frac{Ns}{Nr} * It_{max}$ models. The used parameters are detailed in Tab. 6.

It_{max}	Ns_0	Ns	Nr
500	10000	100	100

Table 6: Tuning parameters of Neighborhood Algorithm.

During the inversion process, low velocity zones were not allowed. The Poisson ratio was inverted in each layer in the range 0.2-0.4 and the density was supposed equal to $2000\,\mathrm{kg/m^3}$ except for the deepest layer ($2400\,\mathrm{kg/m^3}$). Inversions with free layer depths as well as fixed layer depths were performed. 5 layers are enough to explain most of the targets (dispersion and ellipticity), but more layers are used to smooth the obtained results and better explore the parameter space. 5 independent runs of 5 different parametrization schemes (4 and 6 layers over a half space and 14, 15 and 18 layers with fixed depth) were performed. For further elaborations, the best models of these 25 runs were selected (Fig. 15).

The velocity profile is a strong gradient from $300-400\,\mathrm{m/s}$ at the surface increasing rapidly to approximately $1000\,\mathrm{m/s}$ at $30\,\mathrm{m}$. The velocity in the sediments above the bedrock is larger than $1500\,\mathrm{m/s}$. The bedrock depth, generating the ellipticity peak at $0.46\,\mathrm{Hz}$, is poorly constrained around $600 - 800\,\mathrm{m}$. It is in accordance with Fig. 1. Since 2D resonance occurs, the ellipticity data are anyway not reliable. The velocity in the bedrock is not constrained.

When compared to the target curves (Fig. 13), the Love and Rayleigh modes are well reproduced. The predicted increase in the velocity at lower frequency than used in the targets can be seen in the FK plots (Fig. 11). The ellipticity is not perfectly reproduced, but the constraint on the deep layers is anyway very weak.

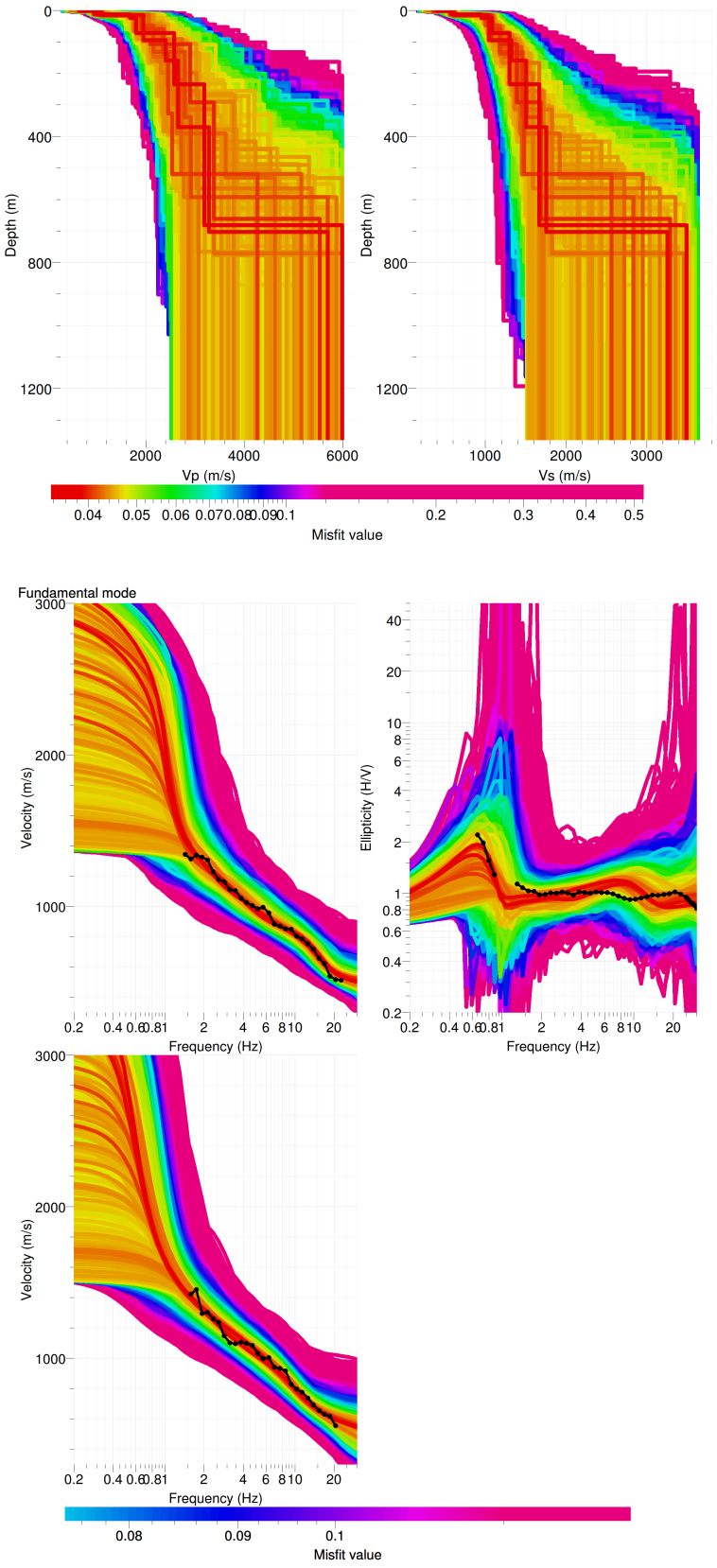

Figure 13: Inverted ground profiles in terms of V_p and V_s (top) and comparison between inverted models and measured Rayleigh and Love modes and corresponding ellipticity, free layer depth strategy.

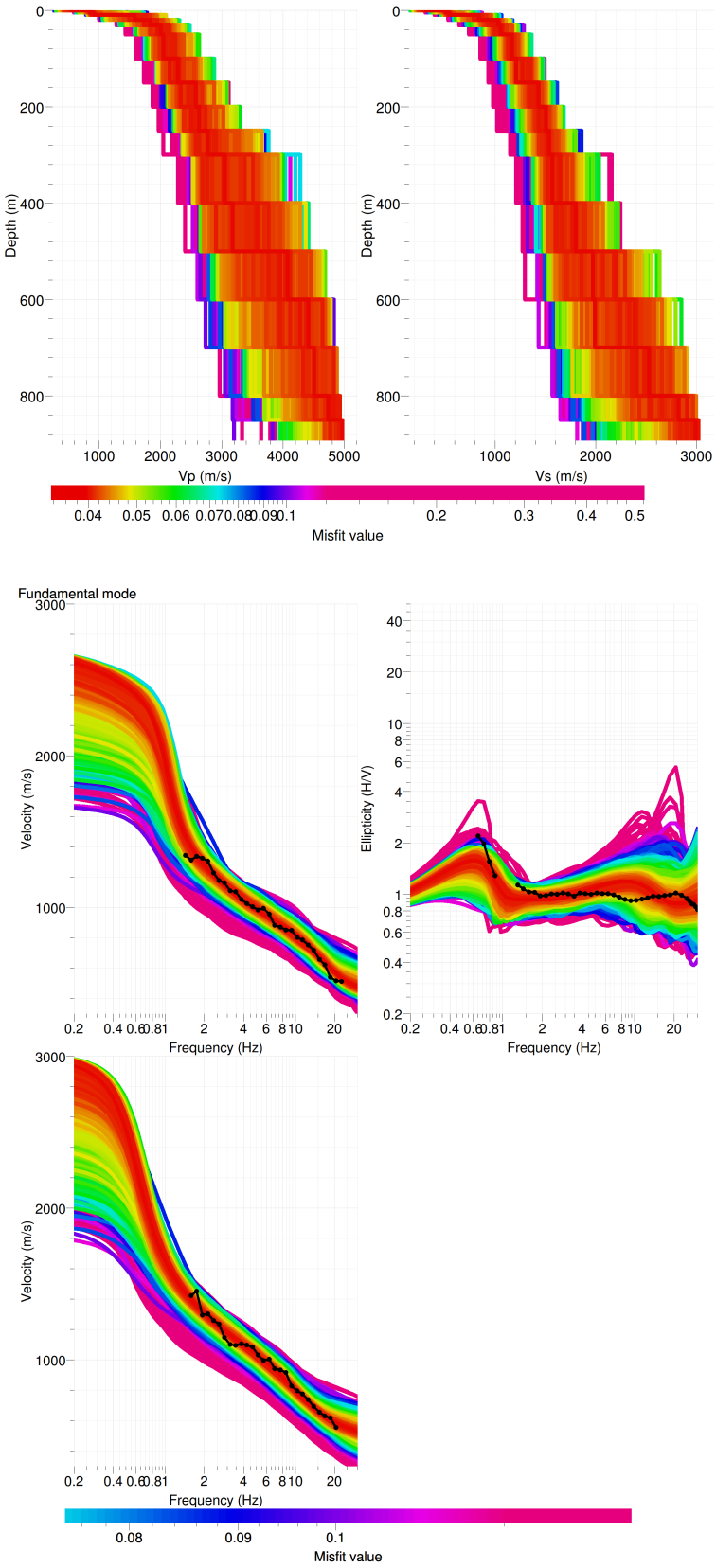

Figure 14: Inverted ground profiles in terms of V_p and V_s (top) and comparison between inverted models and measured Rayleigh and Love modes and corresponding ellipticity, fixed layer depth strategy.

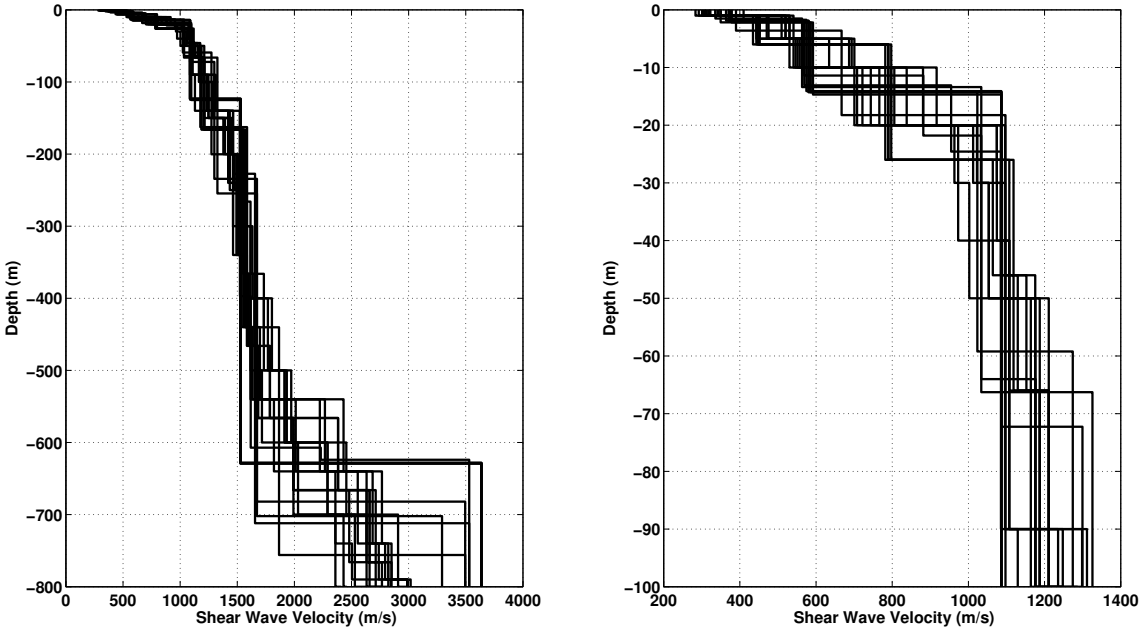

Figure 15: V_s ground profiles for the selected 25 best models (left) and zoom on the 100 first meters.

7.2 Travel time average velocities and soil class

The distribution of the travel time average velocities at different depths was computed from the selected models. The uncertainty, computed as the standard deviation of the distribution of travel time average velocities for the considered models, is also provided, but its meaning is doubtful. $V_{s,30}$ is found to be $714\,\mathrm{m/s}$, meaning the site can be classified as class B in the Eurocode 8 [CEN, 2004] and SIA261 [SIA, 2003]. The map of foundation classes on the website `http://map.bafu.admin.ch/` is providing a class C at this site, which is noticeably different. The sediments in the valley at the station site are more consolidated than expected.

7.3 SH transfer function and quarter-wavelength velocity

The quarter-wavelength velocity approach [Joyner et al., 1981] provides, for a given frequency, the average velocity at a depth corresponding to 1/4 of the wavelength of interest. It is useful to identify the frequency limits of the experimental data (minimum frequency in ellipticity and dispersion curves, 0.65 and $1.5\,\mathrm{Hz}$, respectively). The results using this proxy show that no data is controlling the results below $500\,\mathrm{m}$ and the dispersion curves constrain the results down to nearly $180\,\mathrm{m}$.

Moreover, the theoretical SH transfer function [Roesset, 1970] is computed from the inverted profiles. It is compared to the quarter-wavelength impedance contrast that is a proxy for amplification, that however cannot take resonances into account [Joyner et al., 1981] (Fig. 17). In this case, both approaches match well with a slightly increasing value of amplification from 2 to 3 along the frequencies. This will be compared to observations at this station but is definitely

	Mean (m/s)	**Uncertainty (m/s)**
$V_{s,5}$	450	28
$V_{s,10}$	516	12
$V_{s,20}$	623	11
$V_{s,30}$	714	15
$V_{s,40}$	779	13
$V_{s,50}$	825	12
$V_{s,100}$	960	12
$V_{s,150}$	1042	15
$V_{s,200}$	1119	11

Table 7: Travel time averages at different depths from the inverted models. Uncertainty is given as one standard deviation from the selected profiles.

much lower than expected for the Rhine valley, for example as compared to the Rhone valley (amplifications greater than 5).

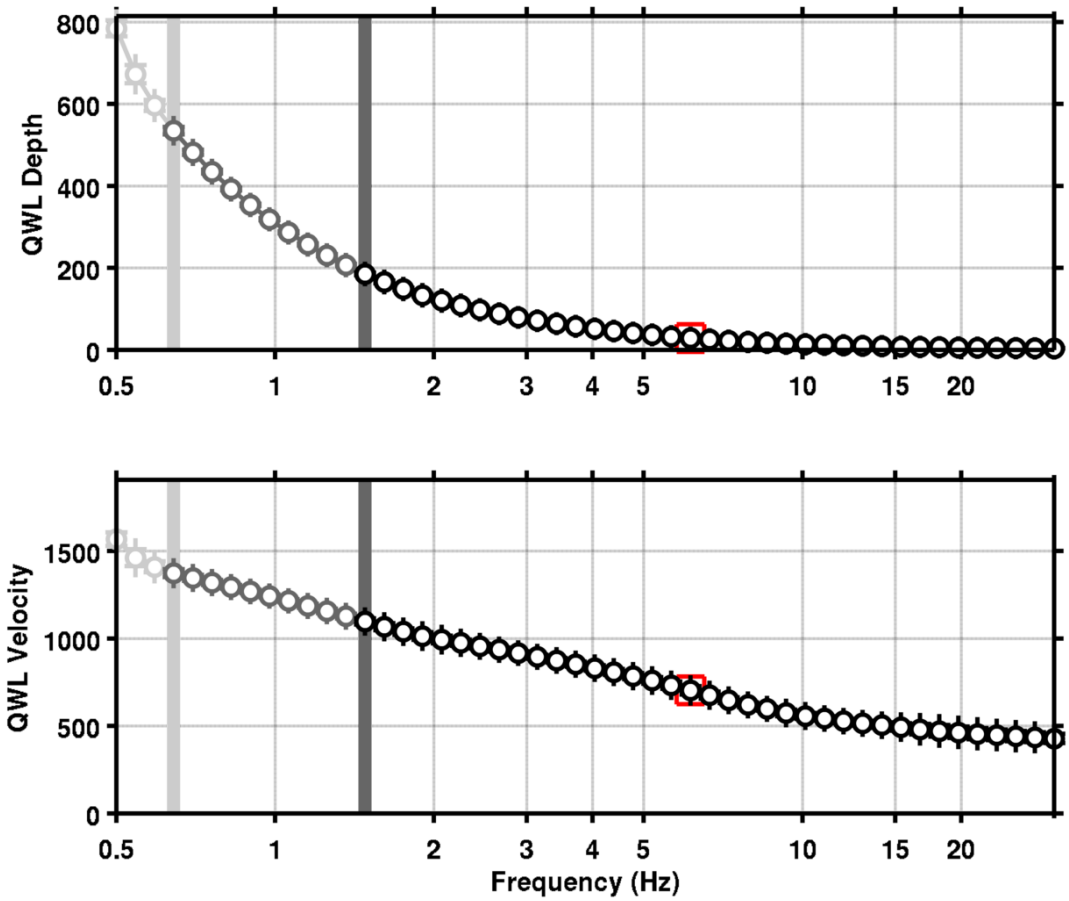

Figure 16: Quarter wavelength velocity representation of the velocity profile. Black curve is constrained by the dispersion curves, grey curve by the ellipticity function, light grey is not constrained by the data. Red square is corresponding to $V_{s,30}$.

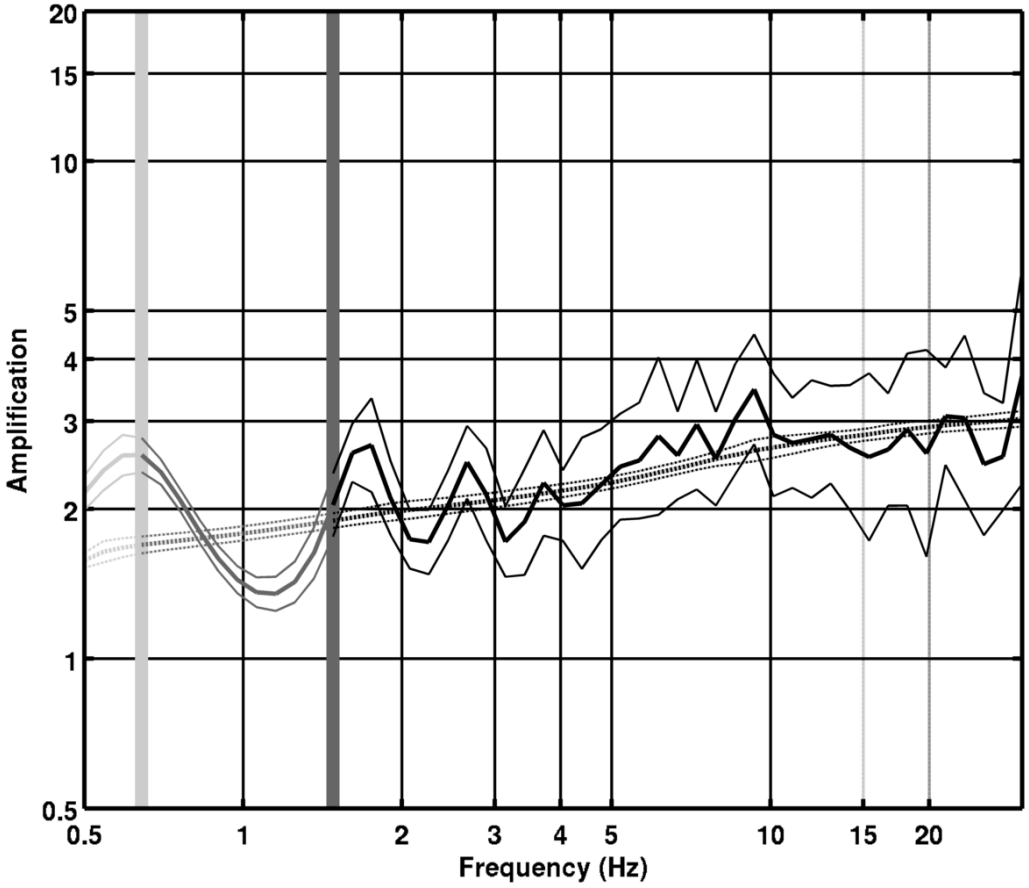

Figure 17: Theoretical SH transfer function (solid line) and quarter wavelength impedance contrast (dashed line) with their standard deviation. Grey scale represents the constraint by the data as in Fig. 16.

8 Conclusions

The H/V survey and polarization analysis showed that the Rhine basin in Chur has a 2D behaviour and that SCUG station is located on the deepest part with a fundamental frequency at $0.46\,\mathrm{Hz}$. The array measurements presented in this study allowed to derive a velocity model below the SCUG station. We found a velocity profile with a strong gradient in the first $30\,\mathrm{m}$ from $300-400\,\mathrm{m/s}$ to approximately $1000\,\mathrm{m/s}$ at $30\,\mathrm{m}$. Below the velocity is increasing up to $1500-2000\,\mathrm{m/s}$ down to the bedrock. The bedrock depth is not well constrained at $600-800\,\mathrm{m}$, much below the constrained part of the profile which reaches still $180\,\mathrm{m}$. $V_{s,30}$ is found to be close to $714\,\mathrm{m/s}$, which is much higher than expected in the Rhine valley. The theoretical SH transfer function and impedance contrast of the quarter-wavelength velocity computed from the inverted profiles support a slightly increasing amplification with frequency with amplitude keeping between 2 and 3. As a conclusion, this inversion is not satisfactory because not enough information is available to constrain the deeper part of the profiles, absolutely necessary to reproduce the observed dispersion. Comparison with transfer functions from earthquakes shows that the profiles may be more complex at depth (velocity inversion?) and can therefore not be simply fixed. In order to improve this, a larger array and/or other measurement types should be used.

Acknowledgements

The author thanks Ivo Egger for the single station measurements, Javier Revilla for the help during the array measurements and Daniel Gilgen and Franz Weber for design of the realtime system.

References

Pierre-Yves Bard and Michel Bouchon. The Two-dimensional resonance of sediment-filled valleys. *Bulletin of the Seismological Society of America*, 75(2):519–541, 1985.

Sylvette Bonnefoy-Claudet, Fabrice Cotton, and Pierre-Yves Bard. The nature of noise wavefield and its applications for site effects studies. *Earth-Science Reviews*, 79(3-4): 205–227, December 2006. ISSN 00128252. doi: 10.1016/j.earscirev.2006.07.004. URL http://linkinghub.elsevier.com/retrieve/pii/S0012825206001012.

Jan Burjánek, Gabriela Gassner-Stamm, Valerio Poggi, Jeffrey R. Moore, and Donat Fäh. Ambient vibration analysis of an unstable mountain slope. *Geophysical Journal International*, 180(2):820–828, February 2010. ISSN 0956540X. doi: 10.1111/j.1365-246X.2009.04451.x. URL http://doi.wiley.com/10.1111/j.1365-246X.2009.04451.x.

J. Capon. High-Resolution Frequency-Wavenumber Spectrum Analysis. *Proceedings of the IEEE*, 57(8):1408–1418, 1969.

CEN. *Eurocode 8: Design of structures for earthquake resistance - Part 1: General rules, seismic actions and rules for buildings*. European Committee for Standardization, en 1998-1: edition, 2004.

Donat Fäh, Fortunat Kind, and Domenico Giardini. A theoretical investigation of average H / V ratios. *Geophysical Journal International*, 145:535–549, 2001.

Donat Fäh, Gabriela Stamm, and Hans-Balder Havenith. Analysis of three-component ambient vibration array measurements. *Geophysical Journal International*, 172(1):199–213, January 2008. ISSN 0956540X. doi: 10.1111/j.1365-246X.2007.03625.x. URL http://doi.wiley.com/10.1111/j.1365-246X.2007.03625.x.

Donat Fäh, Marc Wathelet, Miriam Kristekova, Hans-Balder Havenith, Brigitte Endrun, Gabriela Stamm, Valerio Poggi, Jan Burjanek, and Cécile Cornou. Using Ellipticity Information for Site Characterisation Using Ellipticity Information for Site Characterisation. Technical report, NERIES JRA4 Task B2, 2009.

William B. Joyner, Richard E. Warrick, and Thomas E. Fumal. The effect of Quaternary alluvium on strong ground motion in the Coyote Lake, California, earthquake of 1979. *Bulletin of the Seismological Society of America*, 71(4):1333–1349, 1981.

Katsuaki Konno and Tatsuo Ohmachi. Ground-Motion Characteristics Estimated from Spectral Ratio between Horizontal and Vertical Components of Microtremor. *Bulletin of the Seismological Society of America*, 88(1):228–241, 1998.

Valerio Poggi and Donat Fäh. Estimating Rayleigh wave particle motion from three-component array analysis of ambient vibrations. *Geophysical Journal International*, 180(1):251–267, January 2010. ISSN 0956540X. doi: 10.1111/j.1365-246X.2009.04402.x. URL http://doi.wiley.com/10.1111/j.1365-246X.2009.04402.x.

Frank Preusser, Jürgen M. Reitner, and Christian Schlüchter. Distribution, geometry, age and origin of overdeepened valleys and basins in the Alps and their foreland. *Swiss Journal of Geosciences*, 103(3):407–426, December 2010. ISSN 1661-8726.

doi: 10.1007/s00015-010-0044-y. URL http://link.springer.com/10.1007/s00015-010-0044-y.

J.M. Roesset. Fundamentals of soil amplification. In R. J. Hansen, editor, *Seismic Design for Nuclear Power Plants*, pages 183–244. M.I.T. Press, Cambridge, Mass., 1970. ISBN 978-0-262-08041-5. URL http://mitpress.mit.edu/catalog/item/default.asp?ttype=2\&tid=5998.

Daniel Roten, Donat Fäh, Cécile Cornou, and Domenico Giardini. Two-dimensional resonances in Alpine valleys identified from ambient vibration wavefields. *Geophysical Journal International*, 165(3):889–905, June 2006. ISSN 0956540X. doi: 10.1111/j.1365-246X.2006.02935.x. URL http://doi.wiley.com/10.1111/j.1365-246X.2006.02935.x.

SIA. *SIA 261 Actions sur les structures porteuses*. Société suisse des ingénieurs et des architectes, Zürich, sia 261:20 edition, 2003.

Marc Wathelet. An improved neighborhood algorithm: Parameter conditions and dynamic scaling. *Geophysical Research Letters*, 35(9):1–5, May 2008. ISSN 0094-8276. doi: 10.1029/2008GL033256. URL http://www.agu.org/pubs/crossref/2008/2008GL033256.shtml.